INTERNATIONAL JOURNAL OF CLIMATOLOGY, VOL. 13, 473–495 (1993) 551.521.14:551.588.6(4/9)

GLOBAL LAND-SURFACE ALBEDO MODELLING

CLINTON M. ROWE

Meteorology/Climatology Program, Department of Geography, University of Nebraska-Lincoln, Lincoln, Nebraska 68588-0135, USA

Received 7 August 1991
Accepted 20 July 1992

ABSTRACT

The climatic impact of changes in terrestrial albedo has been studied using numerous climate models, ranging from simple, one-dimensional energy balance climate models to the most complex, three-dimensional general circulation models of the atmosphere. In the majority of these studies, the land-surface albedos have been prescribed both spatially and temporally from albedo observations. The effects of variations in albedo, due to such factors as the angular distribution of incident radiation and plant phenology (especially leaf emergence, senescence, and drop), cannot be deduced from these observation-based albedos.

To overcome the limitations of using observed land-surface albedos in climate models, a model of radiation transfer in plant canopies was used to predict vegetation albedo. This model incorporates the optical properties of the vegetation and soil surface as well as the micro and macrostructure of the canopy. Because of the model's reliance on these physical properties of the land-surface cover, it is able to account explicitly for albedo variations caused by factors both internal and external to the vegetation canopy.

Using the physiognomic classification of natural vegetation developed by Küchler, representative canopy architectures for each of 31 vegetation types were developed for each month of the year. Monthly albedos were then simulated for each vegetation type under a range of irradiance distributions. When these results are compared with existing observations of plant canopy albedo, the degree of correspondence is, in many cases, quite good. Moreover, the dependence of albedo on irradiance distribution predicted by the model agrees well with established theory.

Global maps of land-surface albedo are produced for both clear-sky and overcast conditions in January, April, July, and October using a simple solar radiation model to determine the incident radiation field. These maps are compared with previously compiled maps of land-surface albedo. Large differences between the model- and observation-based global albedo maps occur for each of the four months. However, the model reproduces many of the large-scale features and seasonal trends evident in albedo observations.

KEY WORDS Land-surface albedo Vegetation albedo Global albedo maps

INTRODUCTION

The proportion of incident solar radiation absorbed by the Earth's surface is determined by the surface albedo. A primary determinant of land-surface albedos is the Earth's vegetation cover, which presents numerous absorbing and scattering surfaces to the incident radiation. The interaction of radiation with plant canopies is dependent upon many factors, including the angular distribution and spectral composition of the radiation, the optical properties of the plant foliage, the spatial and angular distributions of the foliage, and the overall architecture of the canopy. Because of these complex dependencies, observations of vegetation albedo are unlikely to represent the full range of possible interactions and, therefore, misrepresent land-surface albedos. In most general circulation models (GCMs), however, land-surface albedo is simply prescribed both spatially and temporally from observations, even though the specification of albedo has been shown to significantly affect model simulations of climate (Charney *et al.*, 1977; Preuss and Geleyn, 1980; Potter *et al.*, 1981; Sud and Fennessy, 1982; Mintz, 1984; Rind, 1984; Dickinson and Henderson-Sellers, 1988; Lean and Warrilow, 1989; Warrilow and Buckley, 1989). Models with prescribed albedos are unable to

0899–8418/93/050473–23$16.50

account for the effects on climate of variations in land-surface albedo due to such factors as the spectral composition and angular distribution of incident radiation, the ratio of direct to diffuse irradiance, plant phenology (especially leaf emergence, senescence, and drop), snow depth and age, and soil moisture. Furthermore, observations of land-surface albedos alone cannot be expected to provide the resolution necessary for climate simulation because of the nature of present observing techniques (Dickinson and Hanson, 1984) and the large range of observed albedos reported in the literature as characteristic of a given surface type (Kukla and Robinson, 1980). Remote sensing techniques can provide estimates of surface albedo only under clear-sky conditions and, except for geostationary satellites, generally provide observations at only one time of day—precluding observation of diurnal variations of surface albedo. Furthermore, because satellite observations are made in narrow spectral bands at fixed viewing angles, transformations from satellite-observed reflectivities to hemispherical albedos must be applied. In addition, atmospheric corrections are necessary to estimate surface albedo from satellite measurements made above the atmosphere. While numerous studies have attempted to derive these transformations and corrections, no standard methodology has been established (Pinker, 1985, 1990). Ground observations can provide data under a wide range of conditions (e.g. both clear and cloudy skies) and can resolve diurnal variations, but give only point estimates of surface albedo. Finally, observation-based albedos cannot be used to investigate climate-albedo interactions. Numerical models of vegetation albedo, therefore, may provide better estimates of land-surface albedos for climate simulations than do observations.

SIMULATING VEGETATION ALBEDO

A model of radiation transfer in vegetation canopies (Kimes and Kirchner, 1982) was modified (Rowe, 1988, 1991) to attempt to overcome the deficiencies of albedo observations. This model incorporates explicitly the optical properties and physical characteristics of a vegetation stand to predict the albedo of the stand under a specified irradiance distribution. The model predicts vegetation albedos that are, in general, different under clear-sky and overcast conditions and it is able to simulate the diurnal variation in albedo caused by changing solar zenith angle (Rowe, 1988, 1991). While Dorman and Sellers (1989) also have developed a model that accounts for albedo variations caused by the distribution of incident radiation and solar zenith angle, their model requires the unnatural assumption of a homogeneous vegetation canopy.

Comparisons of model-predicted albedos with observations demonstrate that the model is able to predict quite well the variation of albedo under different distributions of incident radiation. Differences between modelled albedos and values reported in the literature can be attributed to several factors including: (i) differences in vegetation architecture between the actual canopy and the modelled canopy; (ii) differences between the observed (often unknown or unspecified) and modelled irradiance distributions; (iii) misspecification of foliage dispersion, orientation or optical properties of the modelled canopy; and (iv) incorrect parameterization, especially for sparse vegetation, of the optical properties of the substrate. None the less, the results obtained with the model are encouraging, in part because of the large ranges of observed albedos reported for similar vegetation types (e.g. Kukla and Robinson, 1980; Henderson-Sellers and Wilson, 1983).

Simulations of vegetation albedo were performed (Rowe, 1988) for each of the 31 vegetation types included on Küchler's map of the world's natural vegetation (Küchler, 1978). These results yield estimates of albedo variation as a function of the irradiance distribution at the top of the canopy. The prescribed irradiance distribution was composed of two components: a beam component, which varied from 0 to 100 per cent of total irradiance, and an isotropically distributed diffuse component constituting the remainder. Solar zenith angle was changed from 0° (directly overhead) to 80° (near the horizon).

Model sensitivity to the irradiance distribution (i.e. solar zenith angle and percentage diffuse) was determined for each of the 31 vegetation types for each month of the year. These results are summarized in the following section and the model results are then compared with previously tabulated global albedo data. Additional detail on the specification of vegetation canopy architecture and optical properties, as well as the results of the simulations can be found in Rowe (1988).

Model sensitivity to irradiance distribution

The sensitivity experiment yielded albedo estimates that are, in many respects, consistent with previous observations of the albedo dependence on irradiance distribution. As Henderson-Sellers and Wilson (1983) noted,

> 'for vegetated surfaces, especially where the canopy structure is vertical, minimum albedo occurs when incoming radiation is direct radiation coming from overhead (low zenith) and maximum trapping of radiation by multiple reflection occurs. As the zenith angle increases, the multiple reflection within the canopy decreases, and more radiation is reflected off the top of the canopy.'

This effect is evident in the model results for closed or nearly closed, relatively dense and homogeneous canopies. For relatively sparse vegetation, such as shrub deserts as well as for low-lying vegetation, such as tundra, an opposite trend is apparent. This is because (i) the underlying substrate generally has a higher albedo than does the vegetation and (ii) radiation from near the zenith reaches this substrate more easily than does radiation from near the horizon. The low density of vegetation or its limited vertical development also serves to reduce the importance of light trapping. When vegetation is extremely sparse no trend is apparent and the surface behaves very nearly as a Lambertian reflector. In vegetation with a significant deciduous component, the trend may reverse seasonally as the foliage density changes.

For an isotropic distribution of irradiance, radiation reaches the top of the canopy with an average zenith angle of 60° and thus, for homogeneous canopies, the albedo for isotropic irradiance should be equal to that of beam irradiance at a zenith angle of 60°. While none of the vegetation modules is completely homogeneous, the more nearly homogeneous modules approach this relationship.

While the results outlined above show that the model is able to reproduce observed trends—with respect to solar zenith angle and diffuse irradiance variations—it remains to be demonstrated that the magnitudes are reasonable.

Comparison with previously tabulated albedos

In order to show that the model estimates albedos of the proper magnitude, it is necessary to compare the modelled albedos with those obtained through independent observations. For the model to be validated completely, however, these independently obtained albedo data would need to be accompanied by (i) detailed information on the incident radiation distribution and (ii) descriptions of the vegetation architecture that are sufficient to drive the model. Kukla (1981), in his review of the effects of land-surface albedo on climate variations, recognized that 'existing data are inadequate and incomplete' at least in part because of the lack of details concerning the atmospheric and surface conditions at the time of observation. No entirely adequate validation data set exists and so only less-than-optimal comparisons can be made between modelled and observed albedos.

One of the more complete vegetation albedo data sets compiled to date is that of Matthews (1983, 1984). Her albedo data are given as tabulated, seasonal albedos derived from the literature for each of 32 land-cover categories (29 physiognomic vegetation types plus three non-physiognomic classes) under snow-free conditions (except for permanently snow- or ice-covered surfaces). Direct comparison of these data with the results of the model simulations, however, is difficult for several reasons. First, Matthews' (1983, 1984) land-cover categories are not homologous with those of Küchler (1978). Second, Matthews' data are given seasonally while the present simulations are monthly. Third, Matthews' albedos do not explicitly account for variations caused by solar zenith angle and diffuse irradiance variability. Finally, Matthews (1983) did not completely document her source(s) and so the vegetation and meteorological conditions at the time of observation are not known.

An attempt was made to overcome as many of these difficulties as possible. Each of the 31 Küchler vegetation types was matched to the most closely corresponding formation group of the Unesco (1973) classification (Table I). These were then translated to Matthews' classification system using criteria given by

Table I. Correspondence among Küchler, Unesco and Matthews vegetation classification systems

Küchler	Unesco	Matthews
Tropical rainforest (B)	I.A.1	Tropical evergreen rainforest, mangrove forest
Chaparral (Bs)	I.A.8	Evergreen broadleaved sclerophyllous forest, winter rain
Sonoran desert (Bsp)	III.C.1	Xeromorphic shrubland/dwarf shrubland
Great Basin desert (Bzi, Bz)	IV.C.1	Xeromorphic shrubland/dwarf shrubland
Deciduous forest (D)	I.B.3	Cold-deciduous forest, without evergreens
Caatinga (Di)	I.C.2b	Xeromorphic forest/woodland
Thorn woodland (Ds)	II.C.2b	Xeromorphic forest/woodland
Chihuahuan desert (Dsi)	III.C.2	Xeromorphic shrubland/dwarf shrubland
Saharan desert (Dsp)	III.C.2	Xeromorphic shrubland/dwarf shrubland
Thar desert (Dzp)	IV.C.2	Xeromorphic shrubland/dwarf shrubland
Scrub savanna (DsG)	V.A.3	Tall/medium/short grassland with shrub cover
Savanna woodland (DG)	II.B.1	Tropical/subtropical drought-deciduous woodland
Tropical moist deciduous forest (DBs)	I.B.1	Tropical/subtropical drought-deciduous forest
Needleleaf evergreen forest (E)	I.A.10	Temperate/subpolar evergreen needleleaved forest
Needleleaf evergreen forest—sparse (Ep)	I.A.10	Temperate/subpolar evergreen needleleaved forest
Grassland (G)	V.B.5	Medium grassland, no woody cover
Grassland—sparse (Gp)	V.C.5	Meadow, short grassland, no woody cover
Eucalypt savanna (GBp)	V.A.2a	Tall/medium/short grassland with < 10 per cent woody tree cover or tuft-plant cover
Tree savanna (GD)	V.A.1	Tall/medium/short grassland with 10–40 per cent woody tree cover
Campo (GDp)	V.A.2c	Tall/medium/short grassland with < 10 per cent woody tree cover or tuft-plant cover
Shrub savanna (GDsp)	V.B.3e	Tall/medium/short grassland with shrub cover
Cerrado (GSp)	V.A.2b	Tall/medium/short grassland with < 10 per cent woody tree cover or tuft-plant cover
Tundra (L)	IV.D	Arctic/alpine tundra, mossy bog
Mixed forest (M)	I.B.2	Cold deciduous forest, with evergreens
Needleleaf deciduous forest (N)	I.B.3b(2)	Cold-deciduous forest, without evergreens
Mixed deciduous forest (ND)	I.B.3b(3)	Cold deciduous forest, without evergreens
Semi-deciduous forest (S)	I.A.3	Tropical/subtropical evergreen seasonal broadleaved forest
Monte (Ss)	III.C.1b	Xeromorphic shrubland/dwarf shrubland
Mulga (SsG)	III.C.1a(1)	Xeromorphic shrubland/dwarf shrubland
Patagonian desert (Szp)	IV.C.1b	Xeromorphic shrubland/dwarf shrubland
Mixed semi-deciduous forest (SE)	I.A.9	Tropical/subtropical evergreen needleleaved forest

Matthews (1983). As noted above, there is no one-to-one correspondence between Küchler's and Matthews' and several of Matthews' categories were used repeatedly, while some were never used.

Despite these problems, Matthews' (1983, 1984) albedos are probably the best observation-based data available and so they will be used to assess the validity of the simulated albedos. Additional information on the range of observed albedos for the different vegetation types was obtained from the literature. This search resulted primarily in single albedos, rather than monthly or seasonal albedos, for some of the more common vegetation types. Once again, the vegetation canopy and meteorological conditions at the time of observation usually are not reported. Nevertheless, these albedos should approximate the range of values encountered for a vegetation assemblage (Table II).

Comparison of simulated monthly albedos with the observed albedos can best be made graphically (Figure 1). Because the model estimates the variation of albedo with changing solar zenith angle and percentage diffuse irradiance, the maximum and minimum albedos predicted by the model are shown. These extreme values always occur under conditions of little or no diffuse radiation. For this reason, the simulated albedos under overcast skies (i.e. totally diffuse irradiance) are indicated as well. Seasonal albedos reported by Matthews (1983, 1984) also are plotted for each vegetation type and are supplemented, when possible, by the

Table II. Comparison between observed and simulated albedos

Vegetation Type	Range of observed albedos[a]	Matthews' range	Model range	
			Overall	Diffuse
Tropical rainforest (B)	7·0–18·0	11·0–11·0	7·9–17·0	13·1–13·1
Chaparral (Bs)	13·0–23·0	13·0–17·0	13·6–16·9	15·1–15·4
Sonoran desert (Bsp)	20·0–30·0	28·0–32·0	16·4–20·8	18·8–19·2
Great Basin desert (Bzi, Bz)	20·0–33·0	28·0–32·0	16·4–19·7	17·9–18·0
Deciduous forest (D)	7·0–30·0	12·0–18·0	7·7–19·6	11·2–14·7
Caatinga (Di)		28·0–32·0	5·6–14·2	6·0–11·9
Thorn woodland (Ds)		28·0–32·0	5·3–13·4	5·8–10·1
Chihuahuan desert (Dsi)		28·0–32·0	11·5–16·8	12·7–14·4
Saharan desert (Dsp)	20·0–39·0	28·0–32·0	20·4–23·3	21·9–23·0
Thar desert (Dzp)	20·0–30·0	28·0–32·0	21·4–22·8	22·1–22·6
Scrub savanna (DsG)	10·0–30·0	16·0–25·0	4·4–11·6	6·7–9·8
Savanna woodland (DG)	10·0–30·0	17·0–20·0	8·2–16·8	9·6–15·2
Tropical moist deciduous forest (DBs)		15·0–18·0	7·6–19·0	10·9–13·9
Needleleaf evergreen forest (E)	4·0–27·0	11·0–15·0	7·4–9·9	8·0–8·7
Needleleaf evergreen forest–sparse (Ep)		11·0–15·0	8·8–16·4	9·8–11·8
Grassland (G)	10·0–37·0	16·0–20·0	9·0–26·0	13·8–18·2
Grassland–sparse (Gp)		16·0–20·0	17·3–29·1	17·9–25·9
Eucalypt savanna (GBp)		14·0–16·0	2·8–21·0	14·6–14·9
Tree savanna (GD)	10·0–30·0	14·0–17·0	8·6–18·0	11·8–15·6
Campo (GDp)	10·0–30·0	14·0–16·0	7·7–17·4	13·3–16·2
Shrub savanna (GDsp)	10·0–30·0	16·0–25·0	9·8–21·4	15·8–19·8
Cerrado (GSp)	16·0–24·0	14·0–16·0	9·7–17·2	13·8–15·8
Tundra (L)	10·0–20·0+	12·0–17·0	16·1–20·1	16·5–18·5
Mixed forest (M)		12·0–18·0	6·6–9·5	7·6–8·2
Needleleaf deciduous forest (N)		12·0–18·0	7·4–31·3	8·0–25·0
Mixed deciduous forest (ND)		12·0–18·0	6·2–18·4	7·3–15·0
Semi-deciduous forest (S)		11·0–11·0	9·3–17·6	11·6–13·1
Monte (Ss)		28·0–32·0	16·6–20·5	18·8–18·9
Mulga (SsG)		28·0–32·0	8·1–16·4	13·1–14·1
Patagonian desert (Szp)	20·0–29·0	28·0–32·0	15·2–19·8	17·5–18·1
Mixed semi-deciduous forest (SE)		13·0–16·0	6·5–9·5	7·5–8·2

[a] Sources: Hummel and Reck (1979); Jarvis *et al.* (1976); Kondratyev *et al.* (1982); Lewis and Callaghan (1976); List (1966); Lockwood (1985); Monteith and Unsworth (1990); Oguntoyinbo (1970); Oke (1987); Pinker *et al.* (1980); Posey and Clapp (1964); Rauner (1976); Rauner (1976); Ripley and Redmann (1976); Sellers (1965); Stanhill (1970); Stanhill *et al.* (1966); Stewart (1971).

range of albedos found in the literature. In order to clarify the discussion of all 31 vegetation types that were modelled, they were first grouped into six non-physiognomic classes: forest, shrubland, grassland, tundra, desert, and savanna.

Forest. Ten types of forest are recognized in Küchler's classification and, for the most part, the agreement between the modelled and Matthews' albedos for these vegetation types is quite good. Also, the model results fall within the ranges cited in the literature. Agreement is best for closed forest canopies, such as tropical rainforest, deciduous forest, tropical moist deciduous forest, needleleaf evergreen forest, and semi-deciduous forest. For these forest types, the model appears to predict little seasonal variation in albedo. It must be remembered that the albedos predicted by the model vary depending on the angular distribution of irradiance. Thus, seasonal albedo variation with latitude and solar declination can be predicted, as can the diurnal variation noted by Pinker *et al.* (1980), Pinker (1982) and Henderson-Sellers and Wilson (1983).

Modelled albedos for mixed forest types do not agree well with Matthews' values. This may be, at least in part, due to differences in the relative contributions of the deciduous and evergreen components of the canopies. The modelled canopies likely had a larger proportion of evergreen components, which would serve

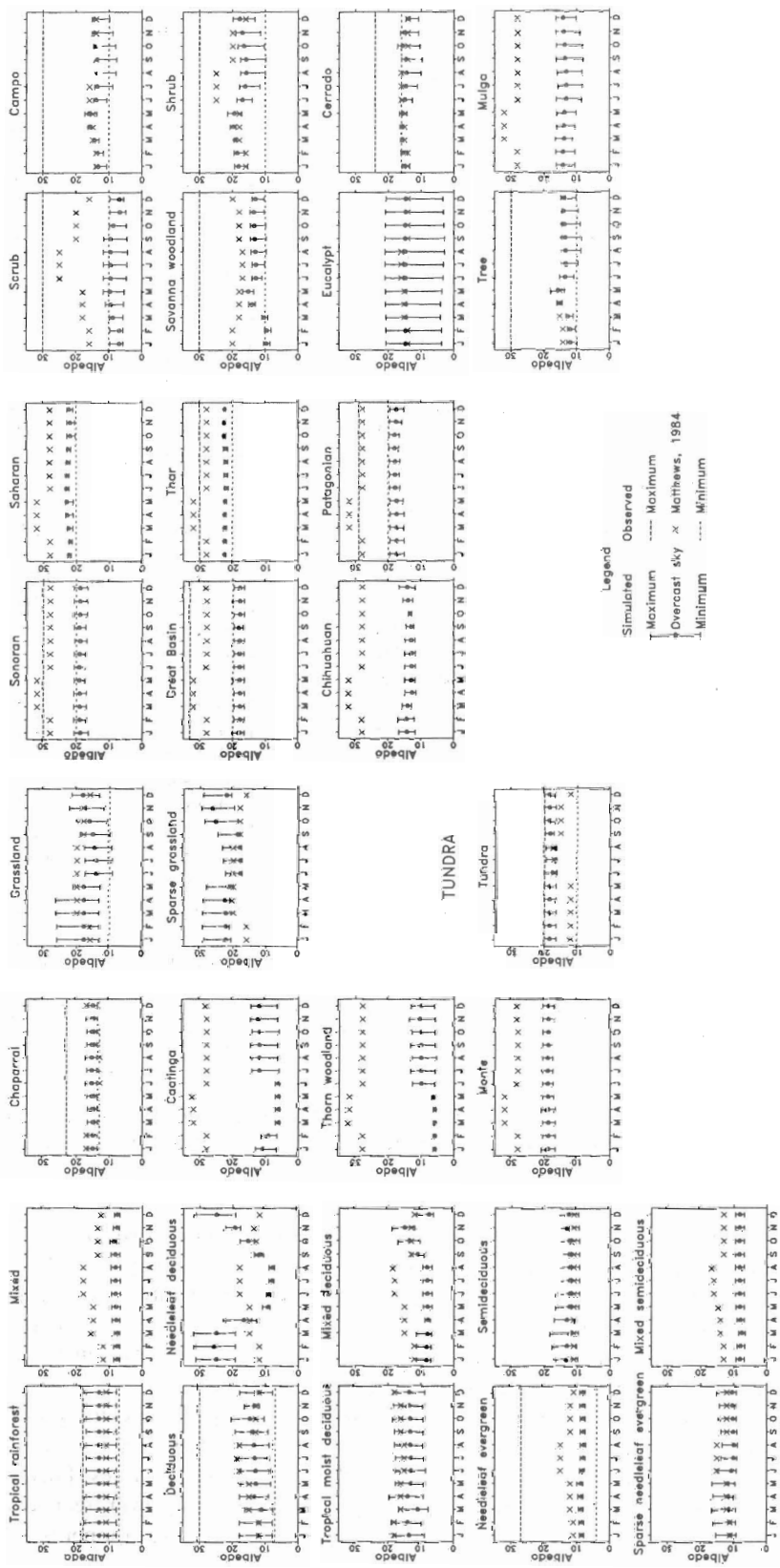

Figure 1. Comparison of modelled monthly albedos for each of Küchler's vegetation types with observed albedos

to reduce the seasonal variation in albedo. The most striking differences are found in those forest types with needleleaf deciduous trees (needleleaf deciduous and mixed deciduous forests). Matthews assigns these forest types to the broad category of 'cold-deciduous forest without evergreens'. This ignores the great physiognomic differences between broadleaf and needleleaf trees. For this reason, the large differences between her values and the simulation results are not surprising. The seasonal variation of albedo produced by the model appears to be representative of the expected seasonality for this vegetation type, since the emergence of new needles in the spring should increase radiation trapping within the canopy and, therefore, yield reduced albedos.

Shrubland. Of the four types of shrubland included in Küchler's vegetation classification, only chaparral has modelled albedos that agree well with Matthews' observation-based values. The three remaining shrublands are more open than chaparral and because of the open nature of the canopy, the specification of the substrate absorption coefficient can have a large influence on simulated albedos. Decreasing the substrate absorption coefficient used in the simulations could easily elevate the modelled albedos to agree with Matthews' values. Without actual soil albedo observations for these regions, this would not be justified. Moreover, Matthews' albedos for these shrublands are the same as her values for vegetation types that correspond to Küchler's deserts and are probably too high for the denser vegetation cover of shrublands.

Grassland. Küchler's grassland category encompasses a wide range of natural vegetation formations. Tallgrass, mixed and short-grass prairies of the USA and Canada, for example, all are classed simply as grassland. Because of their different canopy heights and seasonal growth patterns, different canopy albedos would be expected. These variations cannot be simulated, however, since the architectural differences are masked by Küchler's classification. Model-produced values are within the range found in the literature, but the seasonality differs from that given by Matthews. However, Ripley and Redmann (1975) report a gradual decline in the albedo of a mixed prairie in southern Saskatchewan over the course of the growing season that corresponds to the modelled seasonality. Sparse grass cover allows greater penetration of radiation to the substrate and the model results are higher than for a denser grass cover, but generally exhibit the same seasonal trends.

Tundra. Both Matthews' data and the model-produced results are for snow-free conditions and, thus, are probably representative only of summer conditions in tundra. Model results agree quite well with Matthews' values during this season although they differ considerably during the remainder of the year. It is impossible to explain these differences since Matthews does not reveal how her snow-free tundra albedos were derived from observations.

Desert. For the sparse vegetation of deserts, the value assigned to the substrate absorption coefficient is critical in determining the simulated albedo. The results obtained for deserts are near the minimum albedos found in the literature. Increasing the substrate albedo used in the simulations would increase the predicted albedos. While this would produce better agreement with observed albedos, it cannot be justified on physical grounds. Furthermore, Matthews' albedos for deserts may be too high; in fact, her spring albedos exceed the highest albedos cited in the literature for shrub deserts. Since Matthews applies the same albedos to all shrub deserts, her values do not reflect the variation in albedo that is expected as a result of differences in canopy density, height, and habit (i.e. deciduous or evergreen) between desert types. The effects of these differences are apparent in the modelled albedos for Küchler's six types of desert.

Savanna. Küchler recognizes eight different vegetation types that fall under the rubric of 'savanna'. These vary from a nearly closed woodland with a grass understory to a grassy plain dotted with short trees. Most albedo data sets include only a single category for savanna, but Matthews delimits three classes of savanna that depend on the degree of woody cover. The variable height and coverage of the woody vegetation in savannas should result in a wide range of albedos. As can be seen, the model correctly generates a wide range of albedos, with the lowest values associated with the greatest density of trees and shrubs (e.g. scrub savanna,

savanna woodland, tree savanna, campo, and cerrado). Shrub savanna, which is representative of marginal desert areas such as the Sahel region of Africa, has the highest albedos of any of the savanna types. Both the low density of shrub cover and the reduced grass cover of this vegetation type allow an increase in the amount of radiation reaching the substrate. Agreement between the model results and observations is not good during summer and autumn, but the predicted albedos are well within the range of observations. Eucalypt savanna consists of a relatively open tree canopy high above an understory of continuous grass cover. In essence, there are two separate reflecting surfaces to consider—both of which have predominantly vertical leaves. Vertical leaf-angle distributions have extreme zenith-angle dependencies and this results in a large range of simulated albedos. Overcast sky albedos, which may better represent average daily albedos, agree quite well with Matthews' values for this vegetation type.

GLOBAL LAND-SURFACE ALBEDOS

Results obtained from the simulations of albedo to changes in the above-canopy radiation distribution can be used to produce maps of global snow-free, land-surface albedo. These may then be used to evaluate existing maps of land-surface albedo or to prescribe boundary conditions for climate models.

To derive the geographic distribution to terrestrial albedo, a solar radiation model is required to estimate the above-canopy radiation field. A simple model to estimate the direct and diffuse components of solar irradiance at the top of the canopy is outlined in the next section. The resultant global albedo maps are described and compared with Matthews' (1984) global albedo maps in the subsequent section. Finally, comparisons with the more temporally or geographically limited data sets of Kukla and Robinson (1980), Wilson and Henderson-Sellers (1985), and Dorman and Sellers (1989) are made.

Description of the simple irradiance model

Solar zenith angle and the proportion of total irradiance that is diffuse are needed to estimate the albedo from the tabulations produced in the sensitivity analyses. Earth–sun geometry alone determines the solar zenith angle, but the estimation of the diffuse fraction requires the use of an atmospheric radiation transfer model. Many models are able to estimate accurately the magnitude and angular distribution of solar irradiance at the surface (see, for example, Lacis and Hansen (1974) Stephens (1984), and the review of Davies (1981)). The complexity of these models, however, greatly exceeds the requirements of the present application. Therefore, a very simple solar irradiance model was used to produce estimates of hourly direct and diffuse solar radiation at the surface.

Radiation computations are performed hourly, beginning with solar noon and ending on the hour immediately prior to sunset—by assuming diurnal symmetry, computations for only half the day are necessary. For each hour, the cosine of the solar zenith angle, z, is determined from

$$\cos z = \sin\phi\sin\delta + \cos\phi\cos\delta\cos h \tag{1}$$

where ϕ is the latitude, δ is the solar declination and h is the hour angle—15° for every hour of departure from solar noon. Solar irradiance on a horizontal surface at the top of the atmosphere, Q_s, is

$$Q_s = SV^{-2}\cos z \tag{2}$$

where S is the solar constant (1353 W m^{-2}) and V is the radius vector. Optical air mass (m_o) at sea-level was determined from Kasten's (1966) approximation:

$$m_o = [\cos z + 0{\cdot}15(93{\cdot}885 - z)^{-1{\cdot}253}]^{-1} \tag{3}$$

where z is the zenith angle in degrees. Kasten's equation incorporates the effects of atmospheric curvature and refraction, but must be corrected for locations above sea-level. This adjustment is

$$m_z = m_o(P/P_o) \approx m_o(1 - 9{\cdot}35 \times 10^{-5}E) \tag{4}$$

where P is station pressure (kPa), P_o is standard sea-level pressure (101·3 kPa) and E is station elevation above sea-level (m).

Clear-sky, direct shortwave irradiance at the surface, Q_o, is

$$Q_o = Q_s t^{m_z} \tag{5}$$

where t is the bulk atmospheric transmission coefficient for shortwave radiation. For clear skies, diffuse irradiance, q_o, is

$$q_o = (0{\cdot}91\, Q_s - Q_o)/2 \tag{6}$$

which assumes that 7 per cent of extraterrestrial radiation is absorbed by water vapour, 2 per cent is absorbed by ozone and the remaining 91 per cent is available for atmospheric scattering. Of the scattered radiation, half is assumed to be scattered upward and out of the atmosphere while half is scattered downward toward the surface (List, 1966). The diffuse irradiance reaching the surface is assumed to be distributed isotropically over the sky hemisphere.

Production of global albedo maps

An albedo is first estimated for the direct component of solar irradiance (i.e. zero per cent diffuse irradiance) for the zenith angle determined by the radiation model. Linear interpolation on the cosine of the zenith angle was used to estimate the albedo when the actual solar zenith angle was between the zenith angles included in the albedo model (i.e. 0°, 20°, 40°, 60°, and 80°). Since the albedo model does not include zenith angles greater than 80°, the model-predicted albedo for 80° was substituted directly if the actual zenith angle was greater.

Because diffuse irradiance is assumed to be distributed isotropically over the sky hemisphere, the model-predicted albedo can be obtained by linear combination of the overcast sky (i.e. 100 per cent diffuse irradiance) and beam (i.e. zero per cent diffuse irradiance) albedos. These hourly albedos, weighted by the incident flux, can then be integrated over any time period of interest (e.g. a day).

Several additional assumptions are necessary before global estimates of albedo can be made. Bulk atmospheric transmissivity must be defined for each geographic location at each time step for which irradiance estimates are to be made. For simplicity, bulk atmospheric transmissivity is held constant at 0·6 for the present study (Gates, 1980). This value was chosen so that a range of diffuse proportions would be represented, depending on the optical air mass. For mapping purposes, it was also necessary to assign albedos to regions that receive no shortwave irradiance during part of the year (i.e. poleward of 66°33′ during the winter). These regions were assigned the overcast sky albedo of the appropriate vegetation type.

Hourly clear-sky albedos were estimated on 15 January, 15 April, 15 July, and 15 October for each $1° \times 1°$ grid cell defined as land by the Scripps data set (Gates and Nelson, 1975a, b). These hourly albedos, weighted by the total irradiance for the hour, were integrated over the daylight period to yield daily clear-sky albedos. While this integration removes the diurnal variation of albedo predicted by the model, the seasonal dependence on solar zenith angle is retained, making the model-predicted fields more directly comparable to Matthews' albedos, which do not exhibit any zenith angle dependence. Albedos under completely overcast skies also can be determined from the simulation results by assuming that the radiation incident on the canopy is completely diffuse. Thus, two estimates of snow-free, land-surface albedo—clear-sky and overcast—were produced for each land cell for four times of the year. These were mapped for all locations north of 60°S. Matthews' (1984) seasonal albedos were used in conjunction with her vegetation distribution data set to produce a third set of global snow-free, land-surface albedo maps for January, April, July, and October—the central months of her 3-month seasons. These three sets of global land-surface albedo maps—clear-sky, overcast sky and Matthews'—are described and compared in the following sections.

When comparing these albedo maps, it must be remembered that the geographic distributions of vegetation specified by Küchler (1978) and Matthews (1983, 1984) are significantly different and that these differences affect the resulting spatial variation of albedo.

January albedo. Differences between simulated clear-sky (Figure 2(a)) and overcast (Figure 2(b)) albedos are not large and are restricted to the mid-latitude grasslands of the Northern Hemisphere (e.g. the North American plains and Russian steppes), some savanna regions of South America and sclerophyllous woodland

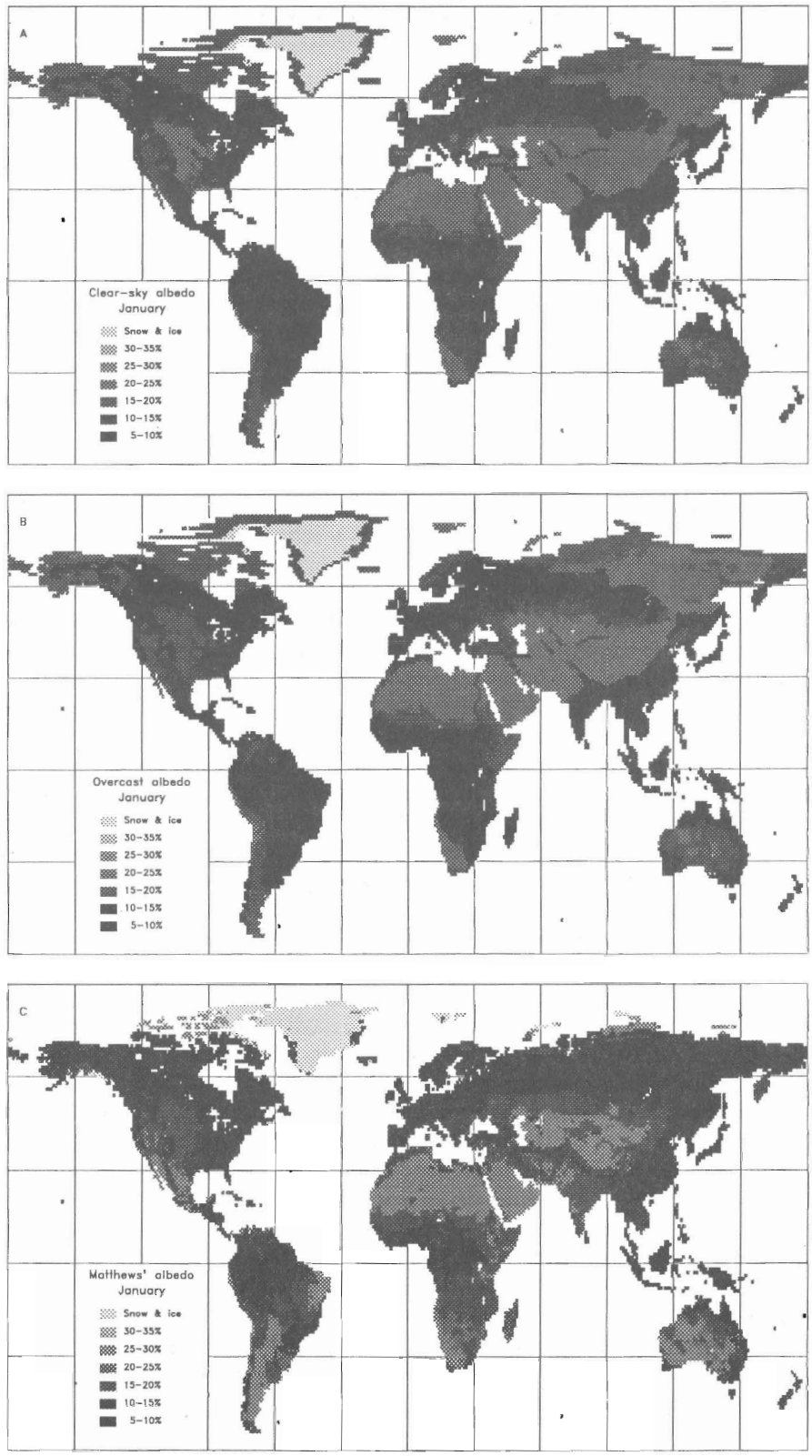

Figure 2. Global albedos for January estimated by the present model for clear (A) and overcast skies (B), and the observation-based albedos reported by Matthews (C)

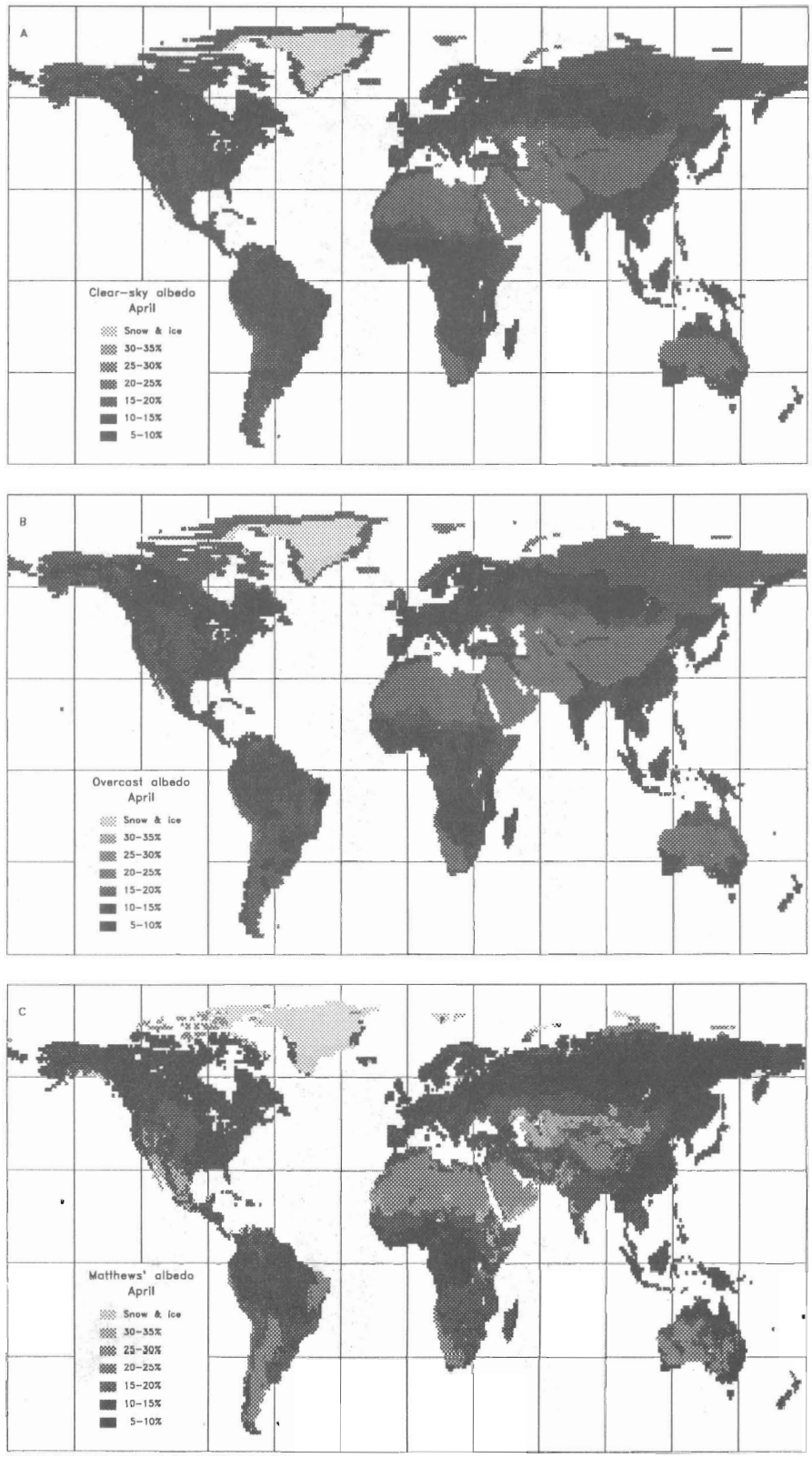

Figure 3. Global albedos for April estimated by the present model for clear (A) and overcast skies (B), and the observation-based albedos reported by Matthews (C)

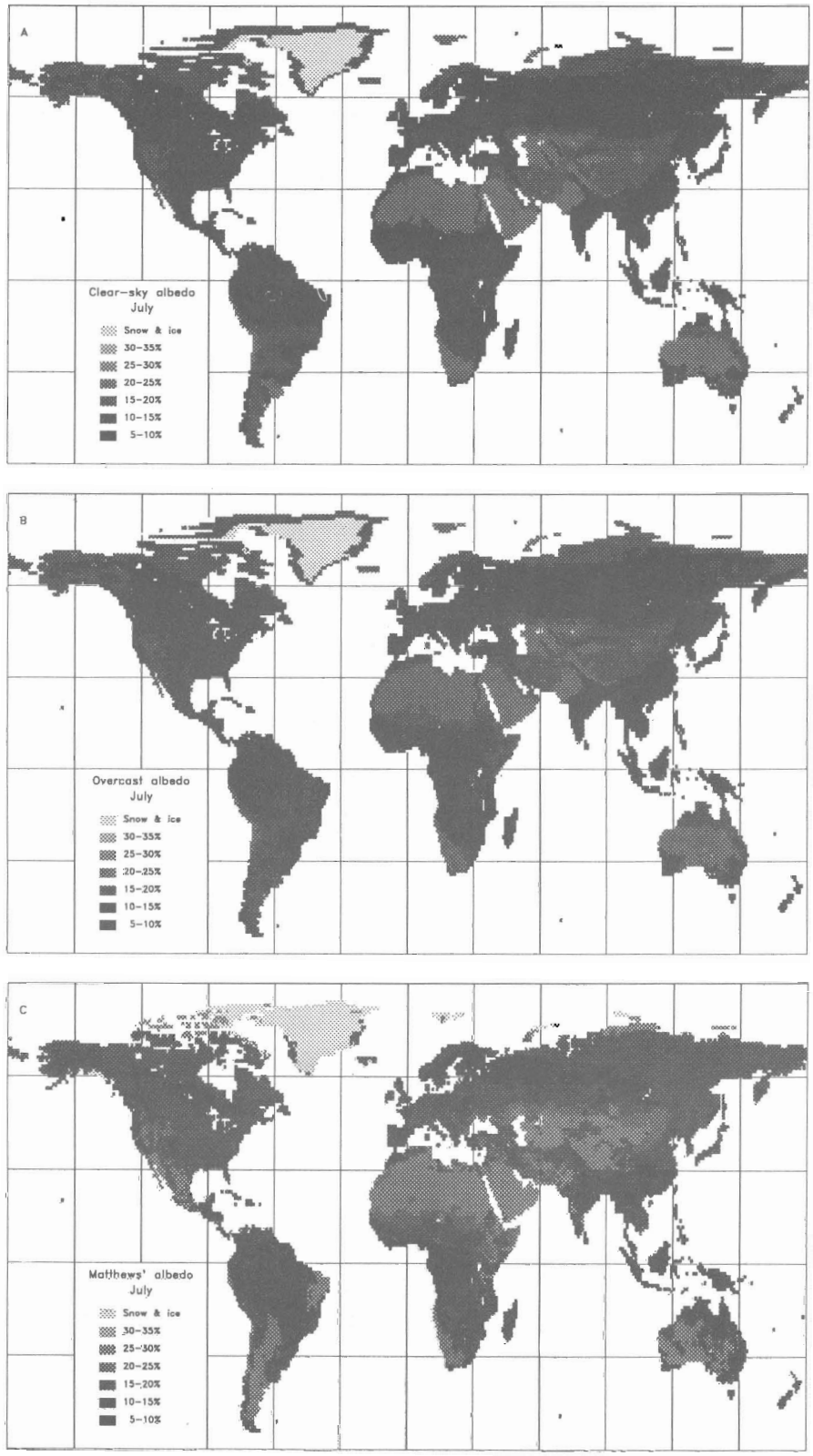

Figure 4. Global albedos for July estimated by the present model for clear (A) and overcast skies (B), and the observation-based albedos reported by Matthews (C)

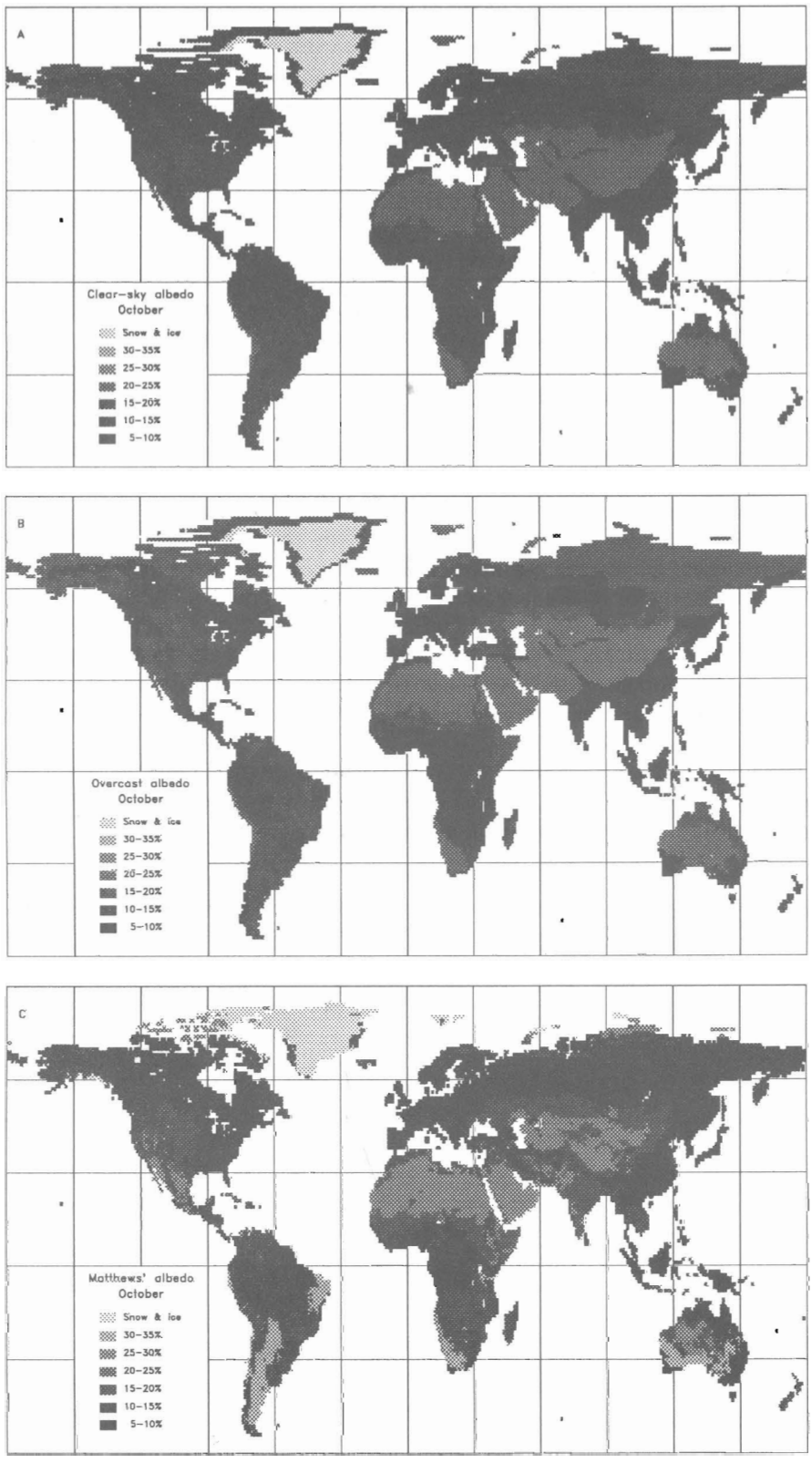

Figure 5. Global albedos for October estimated by the present model for clear (A) and overcast skies (B), and the observation-based albedos reported by Matthews (C)

along the southern coasts of Africa and Australia. Because the mapped clear-sky albedos represent integrated daily values, the zenith angle variation predicted by the model is largely removed and the resulting albedos are close to the overcast sky albedos. This is especially true for the winter hemisphere when diurnal change in zenith angle is minimal.

Maps of the model-predicted land-surface albedos for January exhibit much greater spatial homogeneity than does the map of January albedo based on Matthews' (1984) vegetation and albedo data (Figure 2(c)). This is again in part due to the fact that the model-predicted albedos represent integrations over a range of solar zenith angles. Large differences between model-predicted albedos and Matthews' values occur, for instance, in the needleleaf deciduous forests of central and eastern Siberia and in the Arctic tundra where the sensitivity results do not correspond well with Matthews' seasonal albedo values.

April albedo. Even fewer differences between clear-sky and overcast albedos are apparent in April (Figures 3(a) and 3(b)) and are limited primarily to the semi-deciduous savannas (i.e. 'cerrados') of South America and northern Australia, the grasslands of eastern Africa south and west of Lake Victoria and the central highland grasslands of Madagascar. Once again, this is because integration of clear-sky albedos over the day removes most of the zenith angle dependence.

Seasonal albedo differences are evident, especially in many regions of the Northern Hemisphere. The albedos of the mid-latitude grasslands and needleleaf deciduous forests, for example, have dropped since January, although apparently for different reasons. The change in grassland albedo is due to the changing zenith angle of the sun, since the simulated albedos exhibit a rapid decrease as zenith angle decreases from 60° to 40°. This change is detectable only for clear-sky albedo since overcast albedo does not change in response to solar zenith angle. In contrast, the change occurring in the needleleaf deciduous forest is due to the emergence of new needles, which increases light trapping in the canopy. This effect, of course, decreases both the clear-sky and the overcast albedos.

Once again, large differences can be noted between the model-predicted albedos and those of Matthews (Figure 3(c)) for the reasons cited above. Little seasonal variation is noticeable in Matthews' data and it is limited to increased albedo in only a few small, scattered desert regions.

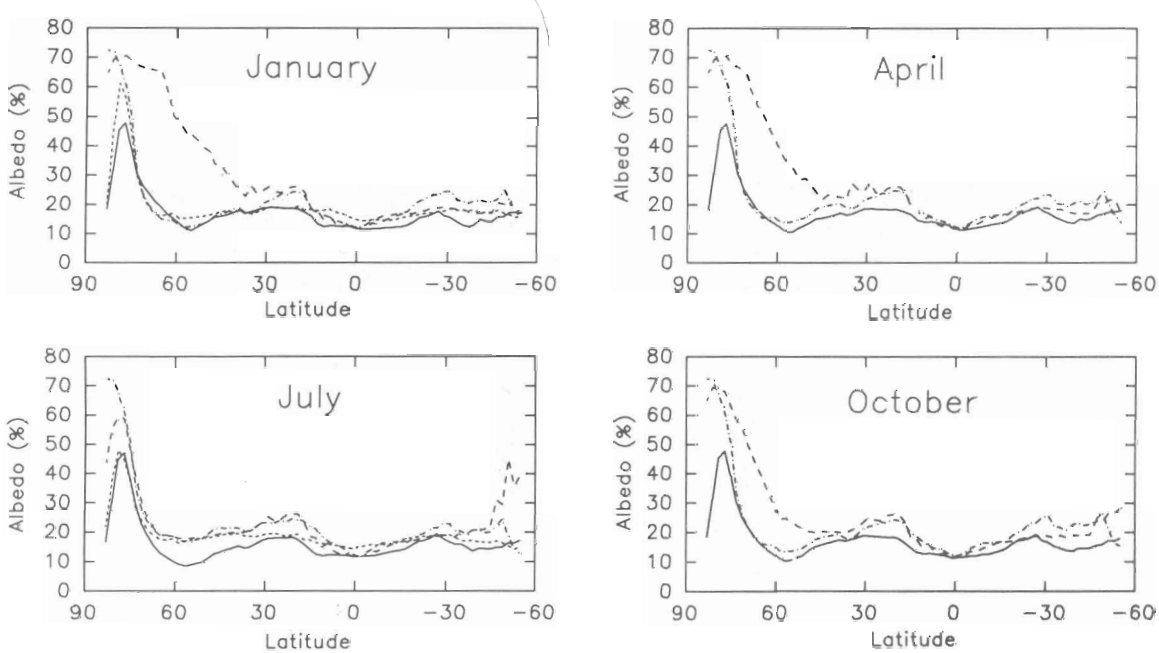

Figure 6. Zonally averaged albedos from the present study (———), Kukla and Robinson (– – –), Matthews (–·–·–), Wilson and Henderson-Sellers (· · · ·)

July albedo. Differences between clear-sky (Figure 4(a)) and overcast (Figure 4(b)) albedo are more extensive in July than in either January or April, occurring over large areas of both hemispheres. The scrub savannas of the Sahel region and the Horn of Africa as well as the semi-deciduous savannas (i.e. 'cerrados') of South America and Australia (between 15°S and the Equator) have higher albedos under overcast conditions. Sclerophyllous woodland (i.e. chaparral or maquis) vegetation in both hemispheres and the Brazilian caatinga exhibit similar trends. An opposite trend—lower albedos for overcast skies—is apparent in the savanna woodlands of southern Africa, the eucalypt savannas of southern Australia and the Southern Hemisphere grasslands, such as the Argentine pampas and the South African veld.

Changes in land-surface albedo from April to July are widespread in response to changing solar geometry and to plant phenology. The albedo of both the Northern Hemisphere mid-latitude grasslands and the needleleaf deciduous forests, for example, continues to decline as the density of foliage increases to its summer maximum. Southern Hemisphere grasslands show an opposite trend from April to July since the foliage density decreases during this period.

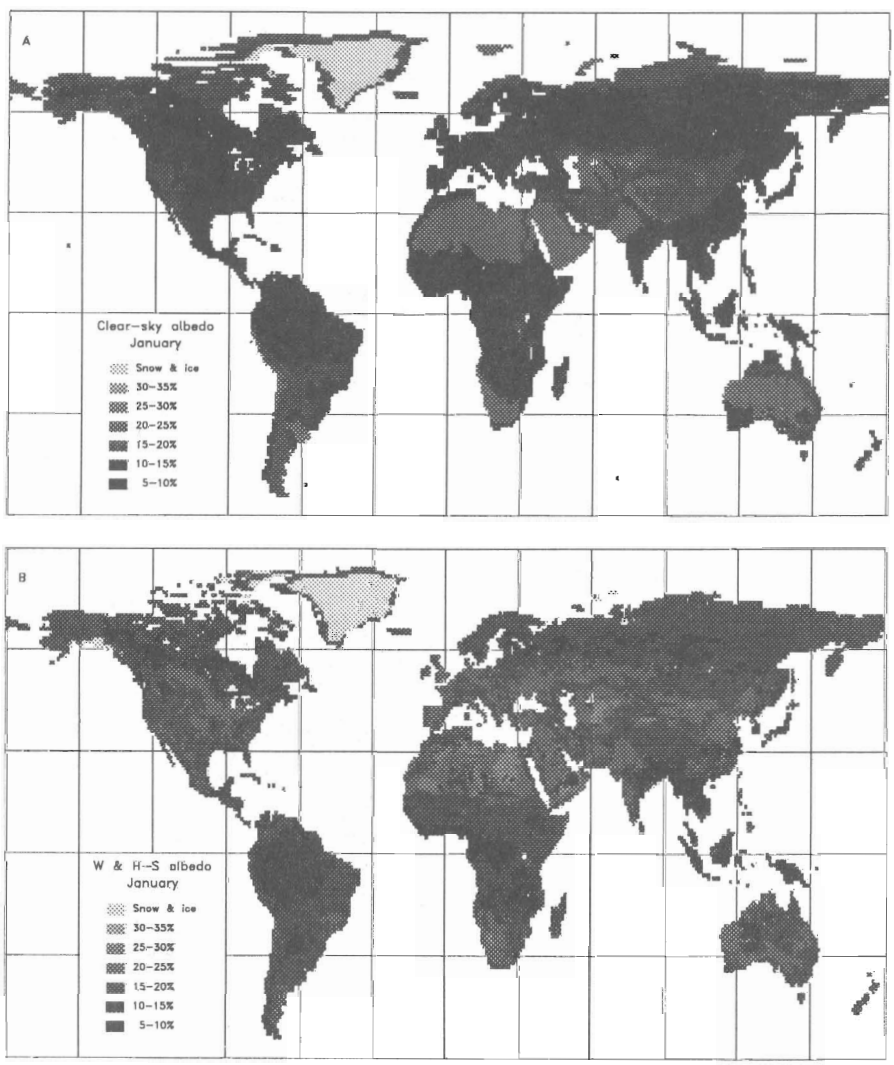

Figure 7. Global albedos for January estimated by the present model for clear skies (A) and the observation-based albedos reported by Wilson and Henderson-Sellers (B)

Matthews' albedos (Figure 4(c)) are nearly everywhere higher than those predicted by either simulation. There are, however, much larger changes in Matthews' albedos between April and July than between January and April—especially in the Northern Hemisphere. This can be attributed to the large summertime albedo increases specified by Matthews for three of the dominant vegetation types of the Northern Hemisphere—deciduous forest, needleleaf evergreen forest and tundra.

October albedo. October exhibits the fewest differences between the clear-sky (Figure 5(a)) and overcast (Figure 5(b)) simulations of any of the four months. Increased albedos under overcast skies are evident in the scrub savanna along the Horn of Africa, the sclerophyllous woodlands of both hemispheres, the semi-deciduous savannas of Venezuela and northern Brazil, the Yucatan thorn forest and the sparse needleleaf evergreen forests of the Kamchatka peninsula. The only region to exhibit a reduced albedo for overcast skies is a small area of deciduous forest in the British Isles.

The prescribed seasonal variation in foliage density of most vegetation types produces very similar canopy architecture in April and October. For this reason, it is not surprising that the global land-surface albedo

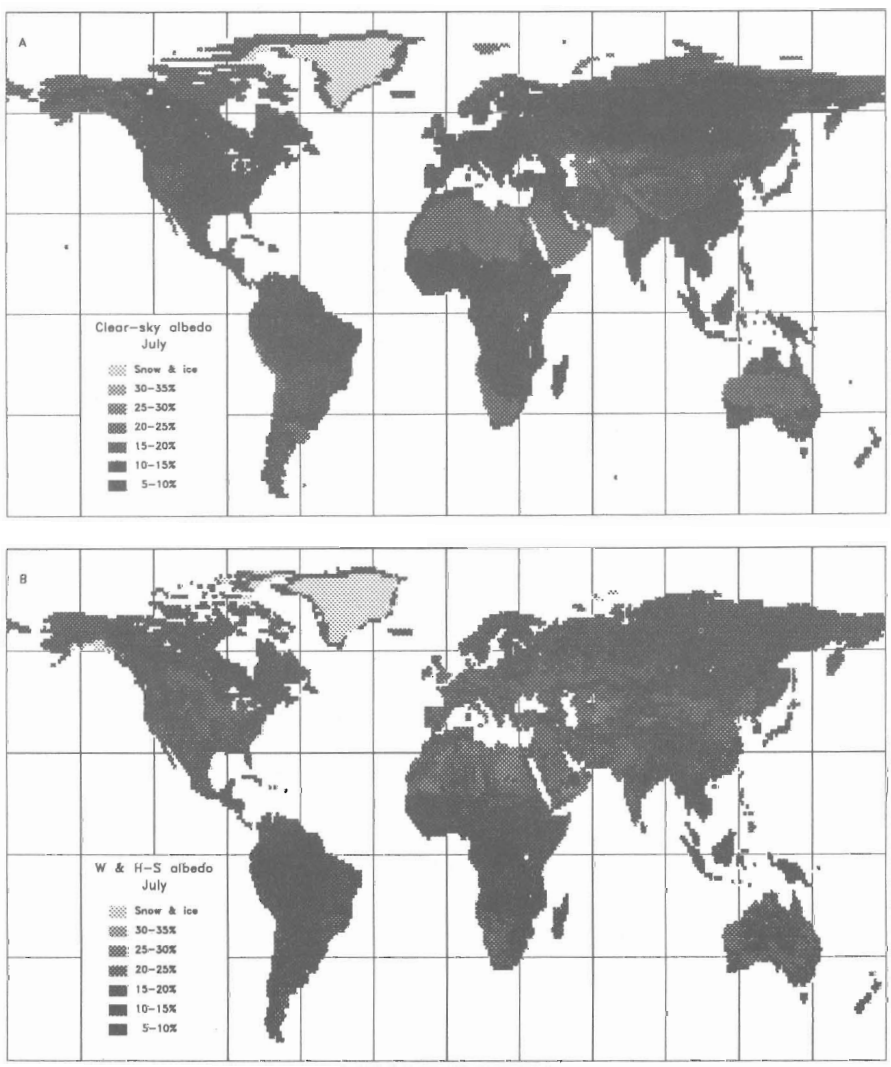

Figure 8. Global albedos for July estimated by the present model for clear skies (A) and the observation-based albedos reported by Wilson and Henderson-Sellers (B)

maps for October closely resemble those for April. This is especially true when considering the simulations for overcast skies, which are not affected by the change in solar declination. Under these conditions, the only differences that can be discerned on the albedo maps are in the Brazilian caatinga and the thorn forests of the northern Yucatan. These drought-deciduous woodlands are found in regions that experience a dry spring and a moist fall and therefore have markedly different foliage densities during these months.

Differences in clear-sky albedo between April and October are confined largely to tropical and subtropical grasslands (e.g. Argentine pampas and South African veld) and savannas (e.g. the semi-deciduous savannas of Brazil, Venezuela and northern Australia and shrub savanna of East Africa) in response to different zenith angles and foliage densities.

The map of Matthews' albedos for October (Figure 5(c)) also closely corresponds to her April albedos since, except for desert areas, her data have only minor differences between spring and autumn. The higher spring albedo prescribed for the desert regions is apparent in the Southern Hemisphere (e.g. the Patagonian, Kalahari, and Australian deserts). This high spring albedo is also evident for the caatinga of north-eastern Brazil.

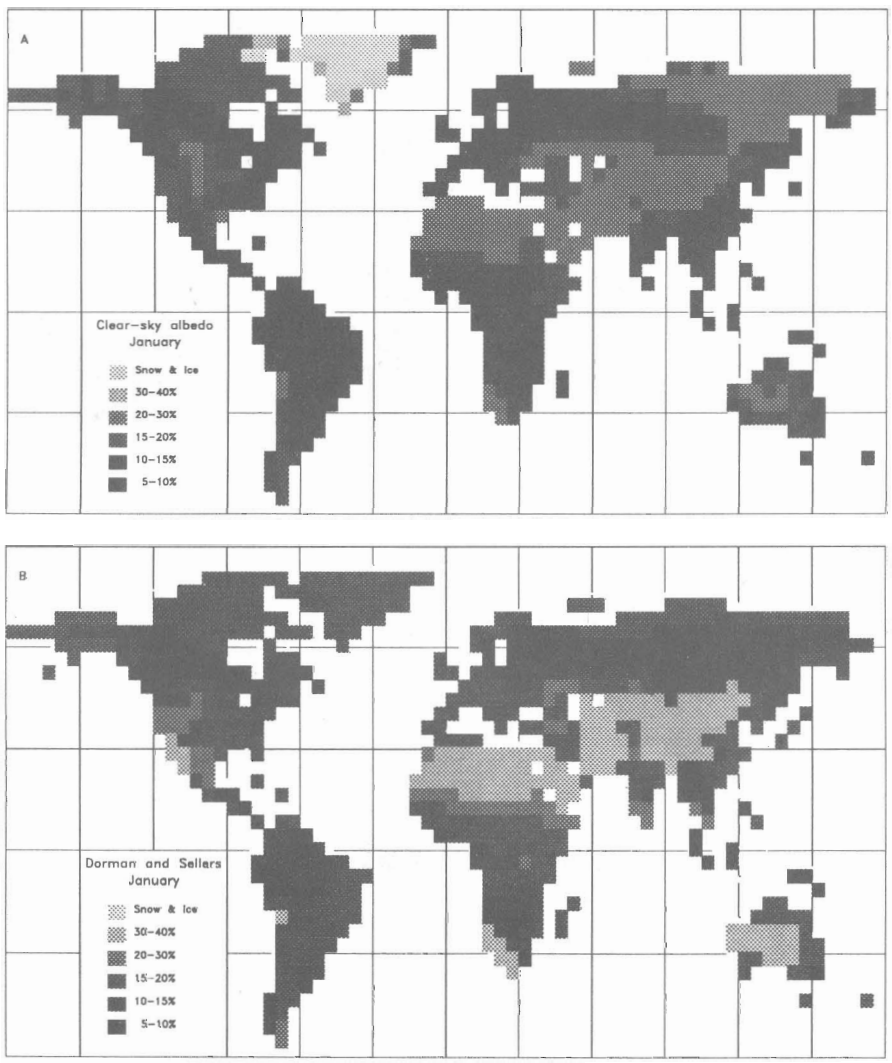

Figure 9. Global albedos under clear skies for January estimated by the present model (A) and the model of Dorman and Sellers (B)

Comparison with other global albedo data sets

While Matthews' (1983, 1984) global albedo dataset is considered to be one of the most comprehensive and accurate representations compiled to date (Dorman and Sellers, 1989), several alternative albedo data sets are available for comparison. The most notable of these are the monthly-averaged, zonal albedos compiled by Kukla and Robinson (1980), the observation-based albedos of Wilson and Henderson-Sellers (1985), and the modelled albedos computed by Dorman and Sellers (1989). Each of these data sets has shortcomings that preclude detailed comparison with the modelled albedos presented here; however, some general comparisons can be made.

Since Kukla and Robinson (1980) presented only zonal averages, the longitudinal distribution of surface albedos is not inherent in their data set. Zonally averaged, land-surface albedos were computed from three gridded albedo data sets (i.e. Matthews, 1984; Wilson and Henderson-Sellers, 1985; and the present study) for comparison with Kukla and Robinson's zonal values (Figure 6). The largest differences occur between Kukla and Robinson's and the other data sets at middle and high latitude of the winter hemisphere, because only

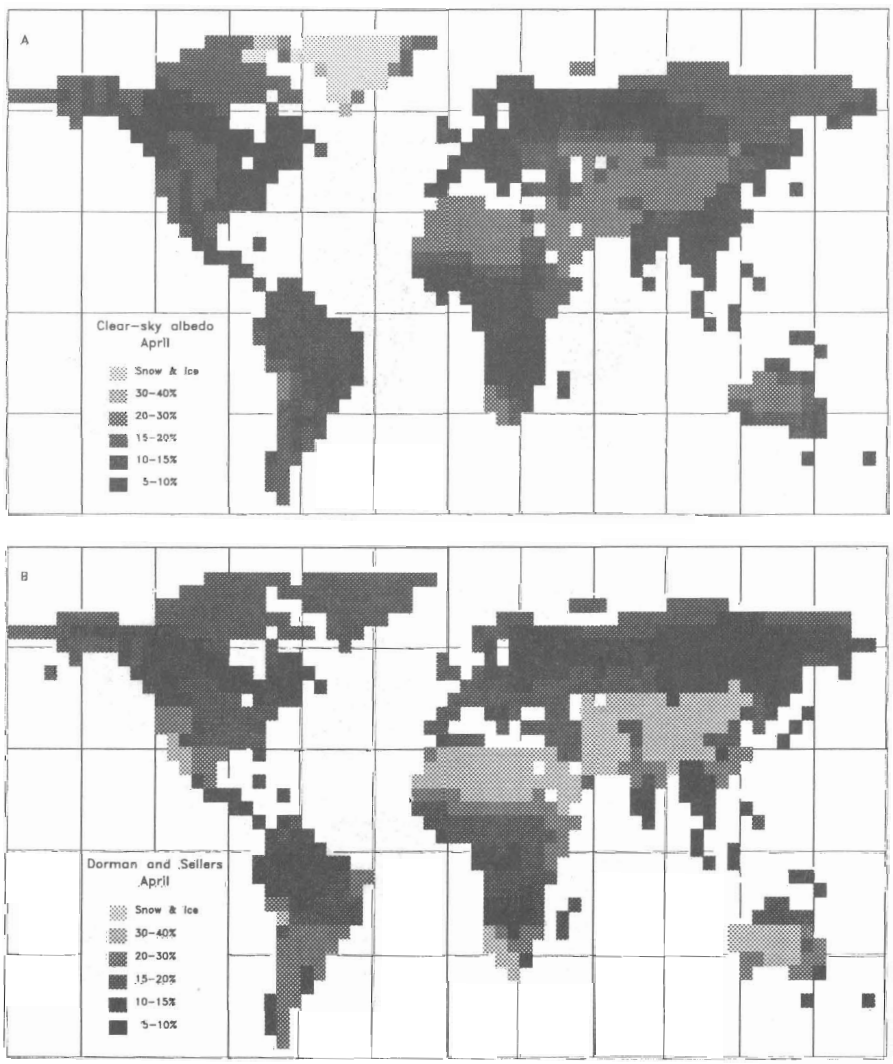

Figure 10. Global albedos under clear skies for April estimated by the present model (A) and the model of Dorman and Sellers (B)

Kukla and Robinson include the effect of snowcover in their compilation. For snow-free conditions, agreement between the model and the three observation-based data sets is quite good. The largest snow-free differences arise in the mid-latitudes of the Northern Hemisphere during summer, when the modelled albedos are significantly lower than all three observation-based albedos. This is a result of the lower albedos for mid-latitude forest predicted by the model. However, not all of the difference can be attributed to errors in the modelled albedos. Indeed, the agreement between the three observation-based compilations is somewhat surprising given the differences in the methodology used to derive them. Kukla and Robinson (1980) use a constant albedo of 17 per cent for all mid-latitude, snow-free regions except semi-deserts and deserts. Wilson and Henderson-Sellers (1985) include the effects of cultivation in their data set, so that much of the mid-latitude forest has been replaced by agricultural lands with generally higher albedos. Finally, as noted above, Matthews (1984) prescribes large albedo increases for both broadleaf deciduous and needleleaf evergreen forests in the summer while the modelled albedos exhibit little change. Furthermore, Matthews does not include a distinct needleleaf deciduous forest type in her compilation, so that large areas of the Northern Hemisphere mid-latitudes are represented as broadleaved rather than needled forests in the summer, resulting in higher albedos at those latitudes.

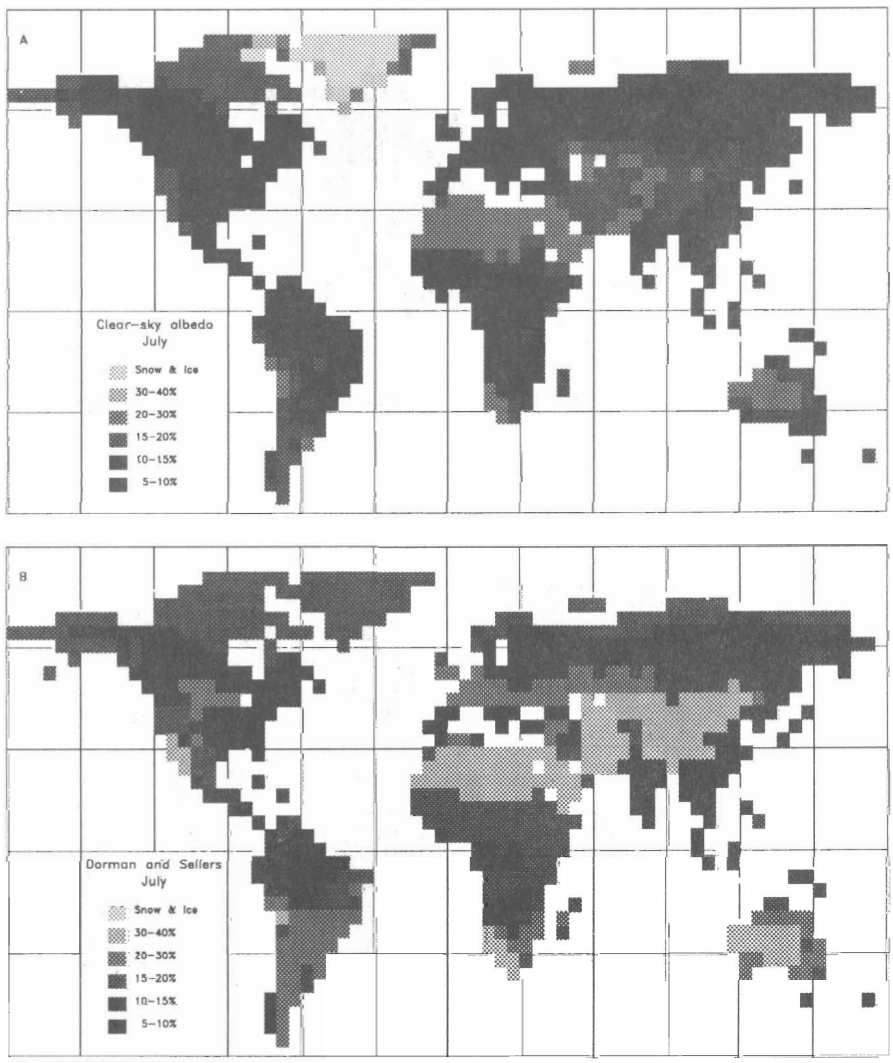

Figure 11. Global albedos under clear skies for July estimated by the present model (A) and the model of Dorman and Sellers (B)

Wilson and Henderson-Sellers' (1985) albedo data set can be assembled on a $1° \times 1°$ grid, although their incorporation of the effects of cultivation makes the comparison with the model results less direct. Moreover, they proposed only summer and winter albedos for each vegetation type, so that comparison can be made only for those seasons (Figures 7 and 8). The most notable features of the Wilson and Henderson-Sellers data set are the small seasonal variation for most regions and the generally greater spatial variation, when compared with either Matthews' data set or the model results. The small seasonal variation is a direct result of the nearly invariant albedos prescribed for most of the land type components used to derive the land-surface albedo for each grid cell (Wilson and Henderson-Sellers, 1985, Table VIII). The greater spatial variation is due to the larger number of land cover classes included in their data set.

Dorman and Sellers (1989) gave their modelled surface albedos for January, April, July, and October—the same months as presented here. However, their results were mapped on to a $4° \times 5°$ grid for presentation. By averaging the surface albedos from the present study for all $1° \times 1°$ land cells in each $4° \times 5°$ grid cell, a rough comparison of the results of these two models can be made (Figures 9–12). While comparisons between models are less valuable than comparison of modelled albedos with observations, they often can serve to

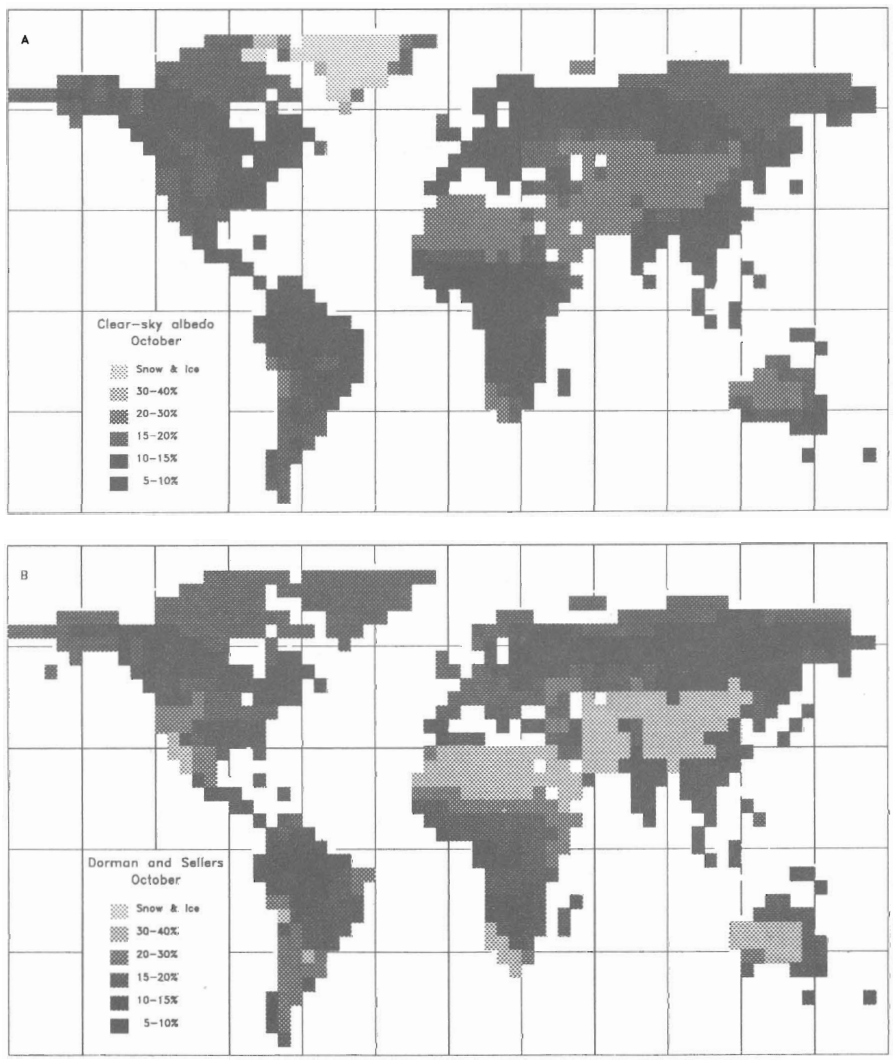

Figure 12. Global albedos under clear skies for October estimated by the present model (A) and the model of Dorman and Sellers (B)

illustrate the differences between the models. In general, Dorman and Sellers' albedos tend to be higher than those predicted here. This result is likely due to the assumption of homogeneous vegetation canopies in Dorman and Sellers' model which would serve to reduce light trapping in the canopy, thus yielding a higher albedo. This effect is especially apparent in the temperate forest and savanna regions. Higher albedos are also apparent in the low-latitude desert regions where Dorman and Sellers replaced Küchler's sparse grass cover type with bare rock and soil. A notable exception to Dorman and Sellers' generally higher albedos is the needleleaf deciduous forests of central and eastern Siberia during winter, spring, and autumn. Dorman and Sellers' model predicts very little seasonal albedo variation for this forest type, even though there is a large change in leaf area index during the year.

SUMMARY AND CONCLUSIONS

A model of radiation transfer in plant canopies was used in an attempt to overcome the deficiencies in using only observations of albedo in climate models. This albedo model explicitly incorporates the optical properties and physical characteristics of a plant stand to predict the albedo of the stand under a specified irradiance distribution. In contrast to other large-scale, observation-based characterizations of albedo, the model predicts vegetation albedos that are, in general, different under clear-sky and overcast conditions. Moreover, the model is able to simulate the well-documented diurnal variation of albedo caused by changing solar elevation. However, simulated albedos often differ considerably from those observed for similar vegetation types. These differences can be attributed to several factors including: (i) differences between the actual vegetation architecture at the time and place of the observation and the architecture of the typical canopy used in the simulation; (ii) the unknown irradiance distribution at the time of the observation; (iii) incorrect specification of foliage dispersion, orientation and optical properties in the model; and (iv) incorrect parameterization, in the case of open canopies, of the underlying surface. Still, the simulation results are encouraging, since overall trends and magnitudes are reasonable and explicable.

Maps of global land-surface albedos were produced for clear-sky and overcast conditions using a simple solar radiation model to determine the above-canopy radiation distribution and are compared with albedo maps produced by other researchers. While large differences between the model- and observation-based global albedo fields are apparent in each month, these differences can be attributed, at least in part, to differences in the vegetation distributions utilized as well as differences in magnitude between the simulated and observed albedos. Nevertheless, the model reproduces many of the large-scale features and seasonal trends evident in the observations.

Modelling of land-surface albedos offers several significant advantages over observation-based albedo data sets for climate modelling. First, the spatial resolution of the model depends primarily on the resolution of the vegetation distribution data and the number of vegetation classes included in the classification. Therefore, updating, modifying and improving the resolution of the modelled albedos will be simpler and faster than the long-term field studies needed to derive observed albedos. Second, the goal of developing interactive biosphere submodels for use in GCMs requires physically based models rather than observation-based parameterizations. Third, climate change studies that include the migration of vegetation zones cannot rely on observation-based albedos, since vegetation albedo depends on solar zenith angle. Finally, modelled albedos include variations caused by irradiance distribution resulting from both seasonal and diurnal changes in solar zenith angle and cloud cover that are not included in current observation-based albedo data sets. While the present model represents an important step in the physically based simulation of vegetation albedo for climate studies, there remains considerable room for improvement, both in the model and in our observations of vegetation architecture and albedo.

REFERENCES

Charney, J. G., Quirk, W. J., Chow, S-M. and Kornfield, J. 1977. 'A comparative study of the effects of albedo change on drought in semi-arid regions', *J. Atmos. Sci.*, **34**, 1366–1385.

Davies, J. A. 1981. *Models for Estimating Incoming Solar Irradiance*, Report No. 81-2, Canadian Climate Centre, Downsview, Ontario.

Dickinson, R. E. and Hanson, B. 1984. 'Vegetation-albedo feedbacks', in Hansen, J.E. and Takahasi, T. (eds), *Climate Processes and Climate Sensitivity*, Geophysical Monograph 29, Maurice Ewing Volume 5, American Geophysical Union, Washington, DC, pp. 180–186.
Dickinson, R. E. and Henderson-Sellers, A. 1988. 'Modelling tropical deforestation: a study of GCM land-surface parameterizations', *Q. J. R. Meteorol Soc.*, **114,** 439–462.
Dorman, J. L. and Sellers, P. J. 1989. 'A global climatology of albedo, roughness length and stomatal resistance for atmospheric general circulation models as represented by the simple biosphere (SiB)', *J. Appl. Meteorol.*, **28,** 833–855.
Gates, D. M. 1980. *Biophysical Ecology*, Springer-Verlag, New York.
Gates, W. L. and Nelson, A. B. 1975a. *A New (Revised) Tabulation of the Scripps Topography on a 1 Degree Global Grid, Part I: Terrain Heights*, R-1276-1-ARPA. The Rand Corporation, Santa Monica, Calif.
Gates, W. L. and Nelson, A. B. 1975b. *A New (Revised) Tabulation of the Scripps Topography on a 1 Degree Global Grid, Part II: Ocean Depths*, R-1277-1-ARPA. The Rand Corporation, Santa Monica, Calif.
Henderson-Sellers, A. and Wilson, M. F. 1983. 'Surface albedo data for climatic modeling', *Rev. Geophys. Space Phys.*, **21,** 1743–1778.
Hummel, J. R. and Reck, R. A. 1979. 'A global surface albedo model', *J. Appl. Meteorol.*, **18,** 239–253.
Jarvis, P. G., James, G. B. and Landsberg, J. J. 1976. 'Coniferous forest', in Monteith, J.L. (ed.), *Vegetation and the Atmosphere*, Vol. 2. *Case Studies*, Academic Press, London, pp. 171–240.
Kasten, F. 1966. 'A new table and approximation formula for the relative optical air mass', *Archiv. Meteorol, Geophys. Bioklimatol., Ser. B*, **14,** 206–223.
Kimes, D. S. and Kirchner, J. A. 1982. 'Radiative transfer model for heterogeneous 3-D scenes', *Appl. Opt.* **21,** 4119–4129.
Kondratyev, K. Ya., Korzov, V. I., Mukhenberg, V. V. and Dyachenko, L.N. 1982. 'The shortwave albedo and the surface emissivity', in Eagleson, P. S. (ed.), *Land Surface Processes in Atmospheric General Circulation Models*, Cambridge University Press, Cambridge, pp. 463–514.
Küchler, A. W. 1978. 'Natural vegetation', in Espenshade, E. B. and Morrison, J. L. (eds), *Goode's World Atlas*, 15th edn, Rand McNally, Chicago, pp. 16–17.
Kukla, G. 1981. 'Surface albedo', in Berger, A. (ed.), *Climate Variations and Variability*, Reidel, Dordrecht, pp. 85–109.
Kukla, G. and Robinson, D. 1980. 'Annual cycle of surface albedo', *Mon. Wea. Rev.*, **108,** 56–68.
Lacis, A. A. and Hansen, J. E. 1974. 'A paramaterization for the absorption of solar radiation in the earth's atmosphere', *J. Atmos. Sci.*, **31,** 118–133.
Lean, J. and Warrilow, D. A. 1989. 'Simulation of the regional climatic impact of Amazon deforestation', *Nature*, **342,** 411–413.
Lewis, M. C. and Callaghan, T. V. 1976. 'Tundra', in Monteith, J. L. (ed.), *Vegetation and the Atmosphere*, Vol. 2. *Case Studies*, Academic Press, London, pp. 399–433.
List, R. J. (ed.) 1966. *Smithsonian Meteorological Tables*, 6th revised edn, Smithsonian Misc. Coll. 114, Washington, DC.
Lockwood, J. G. 1985. *World Climatic Systems*, Edward Arnold, London.
Matthews, E. 1983. 'Global vegetation and land use: new high-resolution data bases for climate studies', *J. Climate Appl. Meteorol.*, **22,** 474–487.
Matthews, E. 1984. 'Vegetation, land-use and seasonal albedo data sets: documentation of archived data tape', *NASA Tech. Memo. 86107*.
Mintz, Y. 1984. 'The sensitivity of numerically simulated climates to land surface boundary conditions', in Houghton, J. T. (ed.), *The Global Climate*, Cambridge University Press, Cambridge, pp. 79–105.
Monteith, J. L. and Unsworth, M. H. 1990. *Principles of Environmental Physics*, 2nd edn, Edward Arnold, London.
Oguntoyinbo, J. S. 1970. 'Reflection coefficient of natural vegetation, crops and urban surfaces in Nigeria', *Q. J. R. Meteorol. Soc.*, **96,** 430–441.
Oke, T. R. 1987. *Boundary Layer Climates*, 2nd edn, Methuen, London.
Pinker, R. T. 1982. 'The diurnal asymmetry in the albedo of tropical forest vegetation', *Forest Sci.*, **28,** 297–304.
Pinker, R. T. 1985. 'Determination of surface albedo from satellite', *Adv Space Res.*, **5,** 333–343.
Pinker, R. T. 1990. 'Satellites and our understanding of the surface energy balance', *Global Planetary Change*, **2,** 321–342.
Pinker, R. T., Thompson, O. E. and Eck, T. F. 1980. 'The albedo of a tropical evergreen forest', *Q. J. R. Meteorol. Soc.*, **106,** 551–558.
Posey, J. W. and Clapp, P. F. 1964. 'Global distribution of normal surface albedo', *Geofis. Internacional*, **4,** 33–48.
Potter, G. L., Ellsaesser, H. W., MacCracken, M. C. and Ellis, J.S. 1981. 'Albedo change by man: test of climatic effects', *Nature*, **291,** 47–50.
Preuss, H. and Geleyn, J. F. 1980. 'Surface albedos derived from satellite data and their impact on forecast models', *Arch. Meteorol. Geophys. Bioklimatol., Ser. A*, **29,** 345–356.
Rauner, Ju. L. 1976. 'Deciduous forest', in Monteith, J. L. (ed.), *Vegetation and the Atmosphere*, Vol. 2. *Case Studies*, Academic Press, London, pp. 241–264.
Rind, D. 1984. 'The influence of vegetation on the hydrological cycle in a global climate model', in Hansen, J. E. and Takahasi, T., (eds), *Climate Processes and Climate Sensitivity*, Geophysical Monograph 29, Maurice Ewing Volume 5, American Geophysical Union, Washington, DC, pp. 73–91.
Ripley, E. A. and Redmann, R. E. 1976. 'Grassland', in Monteith, J. L. (ed.), *Vegetation and the Atmosphere*, Vol. 2. *Case Studies*, Academic Press, London, pp. 349–398.
Rowe, C. M. 1988. *Modeling Land-Surface Albedos from Plant Canopy Architecture*, PhD dissertation, University of Delaware.
Rowe, C. M. 1991. 'Modeling land-surface albedos from vegetation canopy architecture', *Phys. Geogr.*, **12,** 93–114.
Sellers, W. D. 1965. *Physical Climatology*, University of Chicago Press, Chicago.
Stanhill, G. 1970. 'Some results of helicopter measurements of the albedo of different land surfaces', *Solar Energy*, **13,** 59–66.
Stanhill, G., Hofstede, G. J. and Kalma, J. D. 1966. 'Radiation balance of natural and agricultural vegetation', *Q. J. R. Meteorol. Soc.*, **92,** 128–140.
Stephens, G. L. 1984. 'The parameterization of radiation for numerical weather prediction and climate models', *Mon. Wea. Rev.*, **112,** 826–867.

Stewart, J. B. 1971. 'The albedo of a pine forest', *Q. J. R. Meteorol. Soc.*, **97,** 561–564.
Sud, Y. C. and Fennessy, M. 1982. 'A study of the influence of surface albedo on July circulation in semi-arid regions using the GLAS GCM', *J. Climatol.*, **2,** 105–125.
Unesco 1973. *International Classification and Mapping of Vegetation*, Unesco, Paris.
Warrilow, D. A. and Buckley, E. 1989. 'The impact of land surface processes on the moisture budget of a climate model', *Ann. Geophys.*, **7,** 439–450.
Wilson, M. F. and Henderson-Sellers, A. 1985. 'A global archive of land cover and soils data for use in general circulation climate models', *J. Climatol.*, **5,** 119–143.